Zhang et al. *Zool. Res.* 2025, 46(2): 379−387
https://doi.org/10.24272/j.issn.2095-8137.2024.276
https://cstr.cn/32248.14.zr.2024.276

ZR | Zoological Research

Article Open Access

Disentangling the molecular mechanisms underlying yellow body coloration in a soft-shelled turtle

Ju Zhang[1,2,#], Zi-Han Ding[1,3,#], Peng-Fei Wu[1], Wei-Guo Du[1,*], Yue-Qiang Guan[2,*], Xi-Feng Wang[1,*]

[1] *Key Laboratory of Animal Ecology and Conservation Biology*, *Institute of Zoology*, *Chinese Academy of Sciences*, *Beijing* 100101, *China*
[2] *School of Life Science*, *Institute of Life Science and Green Development*, *Hebei University*, *Baoding*, *Hebei* 071000, *China*
[3] *University of Chinese Academy of Science*, *Beijing* 100049, *China*

ABSTRACT

While the functions of body coloration have been well characterized in many animal taxa, the molecular mechanisms governing its production remain poorly understood. This study investigated the genetic and biochemical basis of yellow body coloration in a mutant form of the Yongzhang golden soft-shelled turtle (YGT, *Pelodiscus sinensis*), which exhibit a striking yellow phenotype. Comparative pigment analysis revealed that YGTs have significantly lower melanin and higher carotenoid pigmentation compared to atrovirens wild-type turtles (AWTs), while pterin concentrations did not differ between the two groups. Functional validation experiments demonstrated that a single amino acid substitution (I481R) in tyrosinase-related protein 1 (*tyrp1*) plays a pivotal role in the reduction of melanin production in YGTs. Expression of *tyrp1* from YGTs and AWTs in A375 cells, in which human *tyrp1* (h*tyrp1*) function was depleted by CRISPR-Cas9, led to a specific reduction in melanin production in cells expressing the YGT-*tyrp1* variant. Moreover, *bco1* and *bco2*, genes negatively associated with carotenoid content, showed reduced expression in YGTs, suggesting that yellow coloration is achieved through a reduction in melanin pigmentation combined with an accumulation of carotenoids. These findings elucidate the molecular basis of yellow body coloration in turtles and enhance our understanding of pigment regulation in vertebrates.

Keywords: *Pelodiscus sinensis*; Pigments; Yellow coloration; Molecular mechanisms

INTRODUCTION

Body coloration in animals arises from a complex interplay between structural and pigmentary mechanisms (Cuthill et al., 2017; Shawkey & D'Alba, 2017). Structural coloration results from the interaction of light with microscopic surface structures, generating a variety of colors through physical processes such as refraction, diffraction, and interference (Fu et al., 2016; Saranathan & Finet, 2021). In contrast, pigmentary coloration is determined by pigments, molecules that selectively absorb specific wavelengths of visible light, often localized within specialized pigment cells in vertebrates (Kelsh et al., 2009; Shawkey & D'Alba, 2017). Among these pigment cells, melanophores produce eumelanin and pheomelanin, which are primarily responsible for brown to black coloration, with darker skin, hair, or feathers containing higher concentrations of melanin (McGraw, 2006a). Xanthophores and erythrophores contribute to yellow-to-red coloration through the accumulation of carotenoid and/or pterin pigments (Macedonia, 2000; McGraw, 2006b, 2006c). Both pigment types reflect wavelengths in the yellow to red spectrum and can be deposited within single chromatophores (Schartl et al., 2016). Given the fundamental role of pigments in body coloration, elucidating their contribution is essential for understanding the molecular and cellular mechanisms underlying body color formation in animals.

Melanin pigmentation has been the primary focus of vertebrate coloration genetics, as its underlying genetic mechanisms are well-characterized in model organisms, and the key genes responsible for melanin synthesis are highly conserved across vertebrates (Hoekstra, 2006; Hubbard et al., 2010; McGraw, 2006a). Early research employed candidate gene approaches to identify genes critical for melanin production, such as melanocortin-1 receptor (*mc1r*), tyrosinase (*tyr*), and tyrosinase-related protein 1 (*tyrp1*) (Hubbard et al., 2010; Roulin & Ducrest, 2013; Slominski et al., 2004). More recently, high-throughput sequencing and computational advancements have propelled coloration genetics beyond these candidate gene approaches, permitting the identification of additional genes associated with melanin pigmentation (De Mello et al., 2021; Funk & Taylor, 2019; McLean et al., 2017; Orteu & Jiggins, 2020; San-Jose &

Received: 10 November 2024; Accepted: 11 December 2024; Online: 12 December 2024

Foundation items: This work was supported by the National Natural Science Foundation of China (32030013) and Project of Hebei Agricultural Innovation Team of Freshwater Aquaculture (HBCT2023230204)

[#]Authors contributed equally to this work

*Corresponding authors, E-mail: duweiguo@ioz.ac.cn; guanyueqiang@hbu.edu.cn; wangxifeng@ioz.ac.cn

Roulin, 2017). Nonetheless, the molecular mechanisms and functional validation of genes underlying color production remain largely unexplored in non-model animals, likely due to the limited application of genetic modification technologies in these organisms.

Yellow is a common coloration in vertebrates (Caro & Mallarino, 2020; Cuthill et al., 2017), arising from a variety of pigments (Cloney, 2017; Cooke et al., 2017; Eriksson et al., 2008; Mills & Patterson, 2009; Wolff, 2003). In mammals, pheomelanin is responsible for yellow coat coloration, a phenomenon first described in mice by Silvers and Russell in 1955 (Wolff, 2003). In birds, carotenoid deposition primarily governs yellow skin coloration, observed as early as 1949 in fowl (Eriksson et al., 2008), while a unique class of pigments known as “psittacofulvins” are the predominant determinant of red-to-yellow coloration in parrots (Cloney, 2017; Cooke et al., 2017). Pheomelanin is more prevalent in mammalian and avian pigmentation, whereas carotenoids are the dominant contributors to bright yellow feather coloration in most birds (Elkin et al., 2023; Hubbard et al., 2010; Ito & Wakamatsu, 2003; Roulin & Ducrest, 2013). In contrast, ectothermic vertebrates, including reptiles, amphibians, and fish, achieve yellow-to-red coloration through the accumulation of pteridine or carotenoid pigments, or a combination of both (McLean, 2019; Mills & Patterson, 2009; Macedonia et al., 2000; Merkling et al., 2018; Singh & Nüsslein-Volhard, 2015; Steffen & McGraw, 2007; Weiss et al., 2012).

Despite extensive studies on the biochemical pathways and ecological significance of carotenoid- and pterin-based pigmentation in reptiles (Brejcha et al., 2019; Steffen et al., 2019, 2021; Sun et al., 2024; Zhang et al., 2023), the specific molecular mechanisms regulating yellow coloration remain poorly understood (Andrade et al., 2019; Lu et al., 2024; Recknagel et al., 2024; Tang et al., 2023). As in other vertebrates, reptiles cannot synthesize carotenoids *de novo* and must obtain them from a dietary source (McGraw et al., 2004; Steffen et al., 2019, 2021). Genes involved in carotenoid transport, storage, and metabolism play a critical role in carotenoid-based coloration (McGraw, 2006c). Among them, *bco1* and *bco2,* which encode carotenoid-cleaving enzymes, are key regulators of carotenoid homeostasis (Amengual et al., 2011, 2013). Genetic studies have identified associations among *bco1*/*bco2* function, carotenoid metabolism, and yellow coloration in reptiles (Eriksson et al., 2008; Lehnert et al., 2019; Widjaja-Adhi & Golczak, 2020). Unlike carotenoids, pteridines are synthesized endogenously and contribute to yellow coloration in reptiles (Andrade et al., 2019; Weiss et al., 2012). *Spr*, encoding sepiapterin reductase, is a central gene in pteridine metabolism, catalyzing the biosynthesis of tetrahydrobiopterin and sepiapterin, a yellow pterin (Tian et al., 2024; Ziegler, 2003). Expression analysis has shown that *spr* is significantly downregulated in orange wall lizards, which display high pterin levels, indicating a potential regulatory role in pteridine-based pigmentation (Andrade et al., 2019). In addition to pigment accumulation, reduced melanin production can also produce a yellow phenotype in certain reptiles. For example, in worm lizards (Amphisbaenia), yellow phenotypes result from diminished eumelanin production (Recio et al., 2022). Mutations affecting key melanin biosynthesis genes, such as *tyrp1*, *tyrp2*, *DCT*, and *slc45a2*, have been suggested as potential factors in the development of yellow coloration (Marçon & Maia, 2019; Sun et al., 2024; Tang et al., 2023).

A newly identified bright yellow mutant variant of the Yongzhang golden turtle (YGT, *Pelodiscus sinensis*) (Wang et al., 2022) provides a unique opportunity to investigate the molecular mechanisms underlying yellow body color in turtles. Given the established roles of *tyrp1*, *tyr*, and *tyrp2* in melanin production, *bco1* and *bco2* in carotenoid metabolism, and *spr* in pterin synthesis, these genes were investigated as potential contributors to the YGT pigmentation phenotype. This study characterized the pigment composition of YGTs, assessing melanin, carotenoid, and pterin levels to determine their role in yellow coloration production. A candidate gene approach was employed to analyze *tyrp1*, *bco1*, *bco2*, and *spr* and their involvement in the genetic basis of this phenotype. Results revealed that yellow coloration in YGTs results from a marked reduction in melanin pigmentation accompanied by carotenoid accumulation. A single amino acid substitution in *tyrp1* was identified as a key determinant of decreased melanin synthesis, while down-regulation of *bco1*/*bco2* contributed to increased carotenoid accumulation. These results provide insight into the genetic and biochemical basis of yellow pigmentation in turtles, offering a foundation for further investigations into pigment regulation in vertebrates.

MATERIALS AND METHODS

Animals, tissues, and cell lines

Nine atrovirens wild-type turtles (AWTs) characterized by atrovirens coloration with black spots (Supplementary Figure S1A) and nine YGTs were obtained from Jingtao Turtle Breeding Farms (Fuping, Baoding, China). YGTs represent a newly developed variant of soft-shelled turtle exhibiting a distinct bright golden-yellow coloration (Supplementary Figure S1B) through selective breeding (Wang et al., 2022). Prior to euthanasia, turtles were administered pentobarbital sodium (Euthasol, USA) at a dose of 100 mg/kg via the cloacal mucosa, according to the method described by Ready & Keller (2023). Euthanasia was performed by decapitation to ensure rapid termination, after which the calipash, skin, and muscle were dissected. Collected tissues were immediately flash-frozen in liquid nitrogen and stored at −80°C for subsequent analyses. The human melanoma cell line, A375 (BNCC, China) was maintained in RPMI-1640 medium (Gibco, USA) supplemented with 10% fetal bovine serum (FBS, Gibco, USA) and incubated at 37°C with 5% CO_2 and 95% humidity.

All animal studies and procedures were reviewed and approved by the Animal Care and Use Committee at the Institute of Zoology, Chinese Academy of Sciences (IOZ-IACUC-2023-152).

Determination of melanin content

Melanin content in tissues and cells was determined following a modified protocol based on Hosoi et al. (1985) and Ozeki et al. (1995). For tissue melanin extraction, 10 mg of calipash, skin, and muscle was accurately weighed and placed in 1.5 mL centrifuge tubes with 100 μL of lysate (Solarbio, China), then homogenized for 20 min at 4°C. The homogenate was then centrifuged at 12 000 r/min (centrifugal radius of 6 cm) for 10 min at 4°C, after which the supernatant was discarded. The resulting pellet was dissolved in 3 mol/L NaOH at 80°C for 2 h, followed by absorbance measurement at 500 nm. For melanin quantification in cells, cultures were first washed three times with phosphate-buffered saline (PBS), detached via trypsinization, and centrifuged at 1 000 r/min (centrifugal

radius of 6 cm) at room temperature for 5 min to collect cells. Finally, the cells were solubilized in 3 mol/L NaOH at 80°C for 2 h, with absorbance of the supernatant then measured at 500 nm.

To generate a standard curve, 10 mg of melanin standard (Sigma-Aldrich, Germany) was dissolved in 3 mol/L NaOH at 80°C for 2 h to generate 1 mg/mL standard stock solution. This solution was serially diluted to prepare five working standard solutions at 0.02 mg/mL, 0.04 mg/mL, 0.06 mg/mL, 0.08 mg/mL, and 0.1 mg/mL in 3 mol/L NaOH. Absorbance of these standards was measured at 500 nm, and a standard curve was established (Supplementary Figure S2). Melanin content in tissues and cells was then calculated based on this curve. Each sample measurement was performed in triplicate to ensure reproducibility.

Measurement of carotenoid concentration

Carotenoid concentrations in tissues were determined as described in Grether et al. (2001). Briefly, 0.1 g of accurately weighed tissue (skin, muscle, and calipash) was placed in a 2 mL centrifuge tube with 1 mL of acetone. The tissue was homogenized thoroughly, and the tubes were sealed with aluminum foil and left at 4°C for 24 h. Samples were centrifuged at 8 000 r/min (centrifugal radius of 6 cm) at room temperature for 30 min, after which the supernatant was collected and diluted 10-fold with acetone before spectral analysis. To determine the UV-visible spectra of extracted carotenoids, spectral scanning was performed over the wavelength range of 200–600 nm using a multimode reader (Bio Tek, USA). The extracted yellow carotenoids from the skin, muscle, and calipash of AWTs and YGTs exhibited an absorption peak at approximately 450 nm (Supplementary Figure S3). Finally, absorbance of the diluted supernatant was measured at 450 nm, and the carotenoid concentration was calculated using the formula:

$$W(\text{mg/kg}) = ((A \times \text{K} \times V)/(\text{E} \times G)) \times 10 \quad (1)$$

where A is the measured absorbance, K is a constant (10), V is the volume of the extract (in mL), E is the extinction coefficient of a generic carotenoid (1 cm, 1%) taken as 2 530, and G is the weight of the sample (g).

Measurement of pterin derivatives

Pterin derivatives were extracted and quantified following previously described protocols (Andrade et al., 2019; Gao et al., 2013; Plotkin et al., 2009) with some modifications. Pterin, sepiapterin, and xanthopterin were extracted using 0.05 mol/L NaOH. Briefly, 0.08 g of accurately weighed tissue (skin, muscle, and calipash) was homogenized in 1 mL of 0.05 mol/L NaOH, then subjected to ultrasonic disruption at 50°C for 2 h. The samples were then incubated at 125 r/min in a shaker bath for 1 h and stored at 4°C for 48 h, followed by centrifugation at 10 000 r/min (centrifugal radius of 6 cm) at room temperature for 10 min, with the supernatant collected for further analysis. Standard curves were established for pterin, sepiapterin, and xanthopterin using commercially available standards: pterin (ZZBIO, China), sepiapterin (Psaitong, China), and xanthopterin (SCRSTANDARD, China). Each standard was dissolved in 0.05 mol/L NaOH at a concentration of 10 mg/mL to prepare a working solution, which was subsequently diluted with 0.05 mol/L NaOH to create a concentration gradient series of 0.5, 0.2, 0.1, 0.05, 0.02, and 0.01 μg/μL. All measurements were carried out using an Agilent 1290 Infinity II high-performance liquid chromatography (HPLC) system (Agilent Technologies, USA) equipped with a 4.6 mm×250 mm carbohydrate analysis column (Agilent Technologies, USA). The eluent system consisted of 10 mmol/L Na_2HPO_4 (pH 6) and methanol (19:1) at a flow rate of 1 mL/min for 20 min. Pterin, sepiapterin, and xanthopterin concentrations were calculated based on the HPLC area under 215 nm, 254 nm, and 254 nm respectively. Standard curves for pterin, sepiapterin, and xanthopterin are provided in Supplementary Figure S4A, C, E, while their retention times are shown in Supplementary Figure S4B, D, F, respectively.

Small guide RNA (sgRNA) selection and screening

Knockout (KO) of human *tyrp1* (h*tyrp1*) in A375 cells was achieved using a CRISPR-Cas9-based approach. Five sgRNAs specifically designed to target exon 2, exon 3, and exon 4 of *tyrp1* were selected using the online CRISPR design tool (http://crispr.mit.edu/) (Supplementary Table S1 and Figure S5). Each 20-nt sgRNA, along with its reverse complementary oligonucleotides, was synthesized and annealed by heating at 95°C for 2 min, followed by gradual cooling to 25°C over 45 min to form double-stranded DNA. These annealed oligonucleotides were then cloned into the pX458-Cas9 plasmid, which had been pre-digested with *Bbs* I (NEB, USA) at 37°C for 2 h. Successfully constructed sgRNA-pX458-Cas9 plasmids were purified using the EndoFree Plasmid Maxi Kit (CWBIO, China) before transfection into A375 cells. Lipofectamine 3000 (Invitrogen, USA) was used for transfection following the manufacturer's instructions. Briefly, once the cells in a 6-well plate reached 80%–90% confluence, the growth medium was replaced with 2 mL of complete medium consisting of 90% Opti-MEM and 10% serum. For transfection, two 1.5 mL centrifuge tubes were prepared: one containing 250 μL of Opti-MEM medium and 7.5 μL of Lipofectamine 3000 reagent, and the other containing 5 μg of DNA and 10 μL of P3000™ Reagent. The contents of both tubes were mixed and incubated at room temperature for 15 min before adding 250 μL of the transfection mixture dropwise to each well. Cells were gently agitated and incubated in a 37°C incubator.

Transfected cells were harvested 48 h post-transfection, and genomic DNA was extracted using the UniversalGen DNA Kit (CWBIO, China). Polymerase chain reaction (PCR) primers for the knockout efficiency assessment of sgRNA are listed in Supplementary Table S2. PCR amplification was conducted using PrimerSTAR Max DNA Polymerase (Takara, Japan) with the following cycling conditions: 95°C for 3 min, 35 cycles at 95°C for 10 s, 60°C for 15 s, 72°C for 15 s, and 72°C for 5 min. The resulting PCR products were digested with T7E1 enzyme (NEB, USA) at 37°C for 30 min to analyze sgRNA efficiency. The specific reaction system consisted of 0.25 μL of T7E1, 10 μL of PCR product, 2 μL of 10×NEB Buffer, and ddH_2O to a final volume of 20 μL. Digested products were analyzed by polyacrylamide gel electrophoresis, and editing efficiency was calculated based on band intensity using the following formula:

$$\text{Indel}\ (\%) = 100 \times (1 - (1 - f_{cut})^{1/2}) \quad (2)$$

where f_{cut} is the sum of the grayscale of the cut strip divided by the sum of the grayscale of the total strip.

Generation and validation of CRISPR KO cells

A375 cells were transfected with high-efficiency sgRNAs. At 48 h post-transfection, fluorescence-activated cell sorting

(FACS) was performed using FACSAria III (BD Biosciences, USA) to isolate green fluorescent protein (GFP)-positive clones. Single-cell clones were seeded into 96-well plates at an approximate density of one cell per well and expanded under standard culture conditions. Once the colonies reached confluence in 24-well plates, one-third of the cells from each colony was harvested for genomic DNA extraction using a UniversalGen DNA Kit (CWBIO, China). The PCR products were amplified using detection primers (Supplementary Table S2) under the following conditions: 95°C for 3 min, 35 cycles at 95°C for 10 s, 60°C for 15 s, 72°C for 15 s, and 72°C for 5 min. PCR products were sequenced to confirm successful genome editing.

Plasmid construction and transfection

Total RNA was extracted from the YGTs and AWTs using TRIzol reagent (Takara, Japan), and cDNA was synthesized from 500 ng of total RNA using a PrimeScript™ RT Reagent Kit (Takara, Japan). The coding sequence (CDS) of the *tyrp1* from YGTs and AWTs was amplified using PrimeSTAR Max DNA Polymerase (Takara, Japan) and species-specific primers (Supplementary Table S2) with restriction sites of *Eco*RV and *Not*I (Takara, Japan). The amplified CDS and pcDNA3.1 expression plasmid were digested with *Eco*RV and *Not*I, followed by ligation using T4 DNA ligase (Takara, Japan). All plasmid constructs were confirmed by sequencing (BIG, China).

To assess whether the *tyrp1* (I481R) mutation in YGTs contributes to altered expression and melanin content, h*tyrp1* KO cells were transfected with either YGT-derived *tyrp1* (YGT-*tyrp1*) or AWT-derived *tyrp1* (AWT-*tyrp1*) expression plasmids. Transfections were carried out using Lipofectamine 3000 reagent (Invitrogen, USA) as per the manufacturer's recommendations. After 24 h, melanin was extracted from transfected h*tyrp1* KO cells for subsequent experiments.

Reverse transcription-quantitative real-time polymerase chain reaction (RT-qPCR) analysis of *tyrp1*, *bco1*, *bco2* and *spr*

Total RNA was extracted from tissues and cells using TRIzol reagent (CWBIO, China), and its concentration was determined by measuring absorbance at 260 nm using a Nanodrop 2000 spectrophotometer (Thermo, USA). A total of 1 μg of RNA was transcribed into cDNA using a HiFiScript cDNA Synthesis Kit (CWBIO, China) according to the manufacturer's instructions. Subsequently, qPCR (quantitative real-time PCR) was performed following the instructions provided with the ChamQ Universal SYBR qPCR Master Mix Kit (Vazyme, China) on a LightCycler® 480II Real-Time PCR system (Roche, USA). The amplification reaction was as follows: 95°C for 5 min, 40 cycles at 95°C for 10 s, 55°C for 20 s, 72°C for 15 s, and 72°C for 7 min. Each sample was analyzed in triplicate. The resultant data were analyzed using the $2^{-\Delta\Delta Ct}$ method, with *β-actin* used as an internal reference gene. Primers for qPCR were designed within the coding region of each target gene, and their sequences are provided in Supplementary Table S2.

Statistical analysis

All data were analyzed with GraphPad Prism v.5 (GraphPad Software, USA). Comparisons of pigment content (melanin, carotenoid, and pterin) and the relative expression levels of *bco1*, *bco2*, and *spr* between AWTs and YGTs were performed using unpaired *t*-tests. Statistical significance was set at $P<0.05$, with data presented as mean±standard error (SE). The correlation between *bco1*/*bco2* expression and carotenoid concentration, as well as *spr* expression and pterin/sepiapterin concentrations, was evaluated using Pearson correlation analysis. Initially, a linear regression model was fitted to assess whether a linear relationship existed between gene expression and pigment concentration. Pearson correlation analysis was then applied to quantify the strength and significance of these associations.

RESULTS

Differences in melanin, carotenoid, and pterin derivative concentrations between YGTs and AWTs

Comparative pigment analysis revealed significant differences in melanin and carotenoid pigments between YGTs and AWTs. Notably, AWTs exhibited substantially higher melanin levels in the skin, muscle, and calipash compared to YGTs ($P<0.001$) (Figure 1A). In contrast, carotenoid concentrations were significantly elevated in the skin ($P<0.05$), muscle ($P<0.01$), and calipash ($P<0.01$) of YGTs relative to AWTs (Figure 1B). However, no significant differences were detected in total pterin levels between YGTs and AWTs across all tissues, nor in sepiapterin concentrations in the muscle and calipash ($P>0.05$) (Figure 1C, D). Additionally, AWTs had significantly higher sepiapterin concentrations in the skin than YGTs ($P<0.05$) (Figure 1D). Xanthopterin was undetectable in the skin, muscle and calipash of YGTs, as well as in the skin of AWTs, but was detected in the muscle and calipash of AWTs (Supplementary Figure S6).

I481R substitution reduces melanin content

A mutation in the *tyrp1* coding sequence of YGTs resulted in an I481R substitution (Supplementary Figure S7). To determine whether this substitution contributes to reduced melanin synthesis, a human *tyrp1*-KO (h*tyrp1*) single-cell clone model was established using CRISPR/Cas9 in A375 cells (Figure 2A). Among the designed sgRNAs, target sites 2.1, 2.2, and 4.1 showed high cleavage efficiency (Indel: 2.1=36.5%, 2.2=44.7%, 4.1=40.9%) (Figure 2B). Knockout of h*tyrp1* resulted in a marked decrease in melanin content ($P<0.001$) (Figure 2C, D). Among the hundreds of single-cell clones screened, only 26 GFP-positive clones were obtained. Sequencing of PCR amplicons spanning the target sites confirmed six *htyrp1*-KO clones (2.1-5, 2.2-1, 2.2-7, 4.1-1, 4.1-5, and 4.1-7), all harboring genetic insertions or deletions (Supplementary Figure S8). To assess the functional impact of the I481R substitution, AWT-*tyrp1* and YGT-*tyrp1* were ectopically expressed in h*tyrp1*-null cell clones. Compared to h*tyrp1*-KO cell lines expressing AWT-*tyrp1*, those expressing YGT-*tyrp1* exhibited significantly lower melanin content ($P<0.05$) (Figure 2E).

Differences in *bco1* and *bco2* expression between YGTs and AWTs

Expression patterns of *bco1* and *bco2* varied significantly between YGTs and AWTs across different tissues. For normalization, *bco1* expression in the skin of YGT2 and *bco2* expression in AWT9 were used as relative expression controls (Supplementary Figure S9A, B). Compared to AWTs, YGTs exhibited significantly lower *bco1* expression in the skin ($P<0.05$) and calipash ($P<0.01$) (Figure 3A). Similarly, *bco2* transcript levels were significantly reduced in the skin ($P<0.01$), muscle ($P<0.05$), and calipash ($P<0.01$) of YGTs

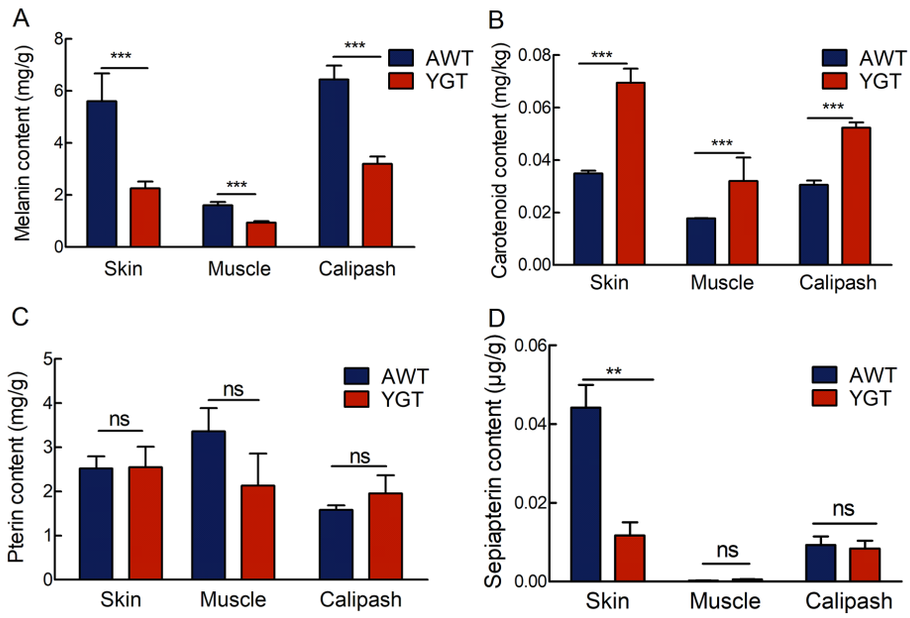

Figure 1 Comparison of melanin, carotenoid, pterin, and sepiapterin concentrations in skin, muscle, and calipash between Yongzhang golden turtles (YGTs) and atrovirens wild-type turtles (AWTs)

A: Melanin concentration in skin, muscle, and calipash of AWTs and YGTs. B: Carotenoid concentration in skin, muscle, and calipash of AWTs and YGTs. C: Pterin concentration in skin, muscle, and calipash of AWTs and YGTs. D: Sepiapterin concentration in skin, muscle, and calipash of AWTs and YGTs. Figure shows mean±SE. ns: Not significant; **: P<0.01; ***: P<0.001.

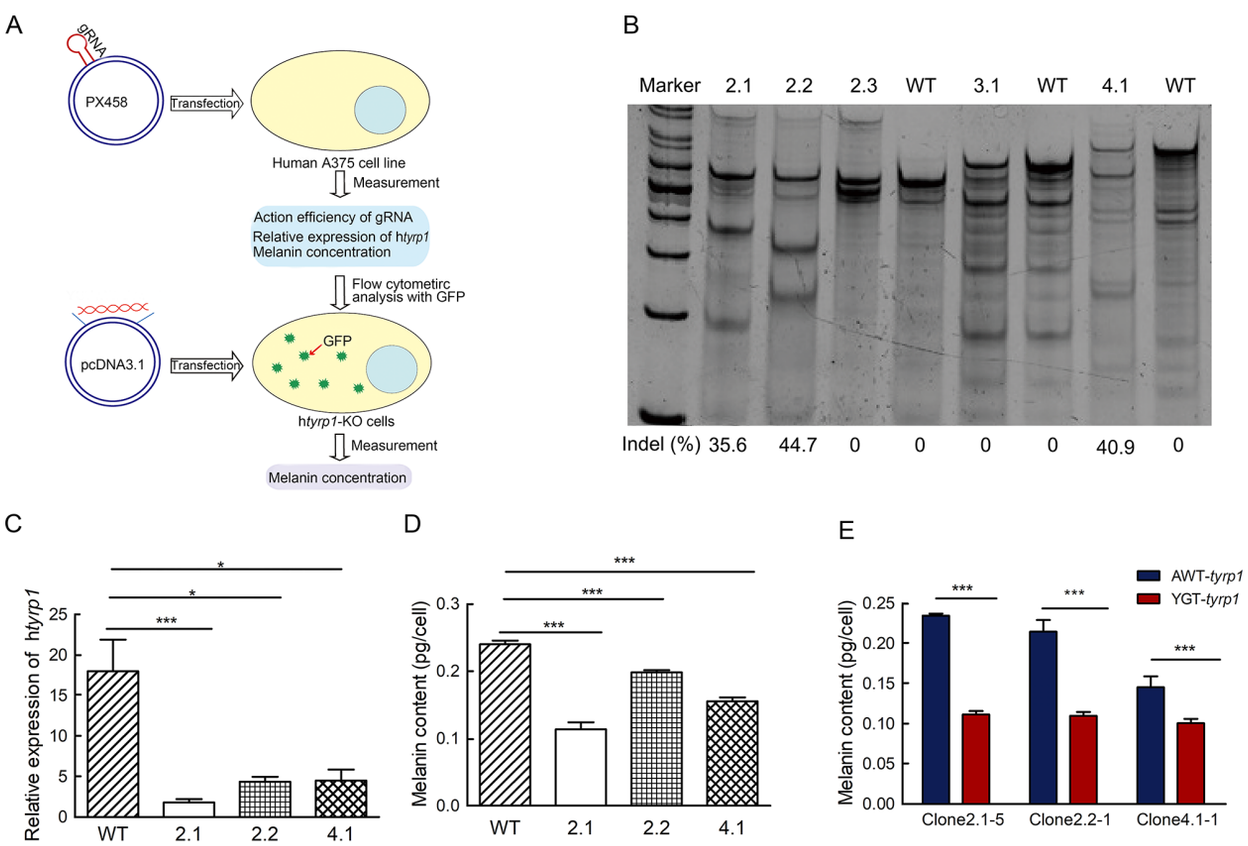

Figure 2 Mutation in *tyrp1* (T1442G) decreases melanin content in YGTs

A: Schematic overview of the methodology used to assess the impact of the *tyrp1* (T1442G) mutation on melanin content in YGTs. A *tyrp1*-knockout (h*tyrp1*-KO) human melanoma cell line was first generated using CRISPR-Cas9 in A375 cells, followed by monoclonal cell selection by flow cytometry. h*tyrp1*-KO cells were transfected with either YGT-*tyrp1* or AWT-*tyrp1*, and melanin content was quantified. B: Evaluation of editing efficiency for sgRNAs sg2.1, sg2.2, sg2.3, sg3.1, and sg 4.1, with indel efficiency calculated based on band intensity. C: Relative expression of h*tyrp1* in A375 (WT) and h*tyrp1*-KO cells. Clones 2.1, 2.2, and 4.1 correspond to *htyrp1*-KO cells generated using sgRNAs g2.1, g2.2, and g4.1, respectively. D: Melanin concentration in WT cells and h*tyrp1*-KO cells, with clones 2.1, 2.2, and 4.1 generated using sgRNAs g2.1, g2.2, and g4.1, respectively. E: Melanin concentration in h*tyrp1*-KO monoclonal cells expressing YGT-*tyrp1* or AWT-*tyrp1*. *: P<0.05; ***: P<0.001.

relative to AWTs (Figure 3B).

Negative correlation between *bco1*/*bco2* expression and carotenoid concentration

Carotenoid concentration showed a strong negative correlation with *bco1*/*bco2* expression across multiple tissues in both YGTs and AWTs (Figure 4). In the skin, muscle, and calipash, correlation coefficients (R) between carotenoid concentration and *bco1* expression were –0.5795 and –0.3815, –0.8765 and –0.6695, and –0.3750 and –0.8346 for AWTs and YGTs, respectively (Figure 4A–C). Similarly, correlation coefficients (R) between carotenoid concentration and *bco2* expression in the skin, muscle, and calipash of AWTs and YGTs were –0.713 and –0.3283, –0.7992 and –0.6999, and –0.5577 and –0.5287, respectively (Figure 4D–F).

Negative correlation between *spr* expression and sepiapterin concentration in skin and calipash

To assess *spr* expression, the relative expression control was set using *spr* levels in the skin of AWT1 (Supplementary Figure S9C). No significant differences were observed in *spr* expression between YGTs and AWTs in skin and muscle (P>0.05). However, *spr* expression was significantly higher in the calipash of YGTs compared to AWTs (P<0.05) (Figure 5). Furthermore, sepiapterin concentration showed a significant negative correlation with *spr* expression in the skin and calipash of YGTs and AWTs (Supplementary Figure S10D, F). In contrast, no correlation was detected between *spr* expression and pterin concentration in the skin, muscle, or calipash of YGTs and AWTs (Supplementary Figure S10).

DISCUSSION

Yellow coloration is widespread among reptiles (Andrade et al., 2019; Olsson et al., 2013), yet the specific molecular mechanisms underlying its production remain largely unexplored across many taxa (Andrade et al., 2019; McLean et al., 2017; Steffen & McGraw, 2007, 2009). This study demonstrated that the bright yellow pigmentation in YGTs resulted from a combination of reduced melanin synthesis and increased carotenoid accumulation, mediated by alterations in genes responsible for producing melanin (*tyrp1*) and degrading carotenoid-based pigmentation (*bco1* and *bco2*). Specifically, a mutation in *tyrp1* impaired melanin production,

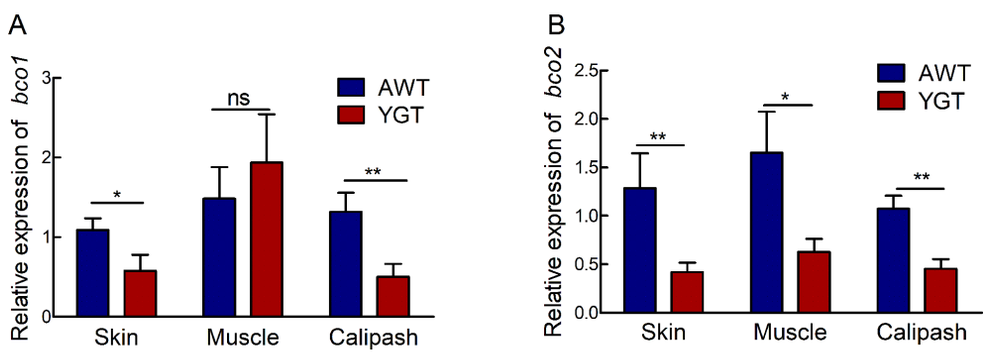

Figure 3 Comparison of relative expression of *bco1* and *bco2* in skin, muscle, and calipash between Yongzhang golden turtles (YGTs) and atrovirens wild-type turtles (AWTs)

A: Relative expression of *bco1* in different tissues of AWTs and YGTs. B: Relative expression of *bco2* in different tissues of AWTs and YGTs. Figure shows mean±SE. ns: Not significant; *: P<0.05; **: P<0.01.

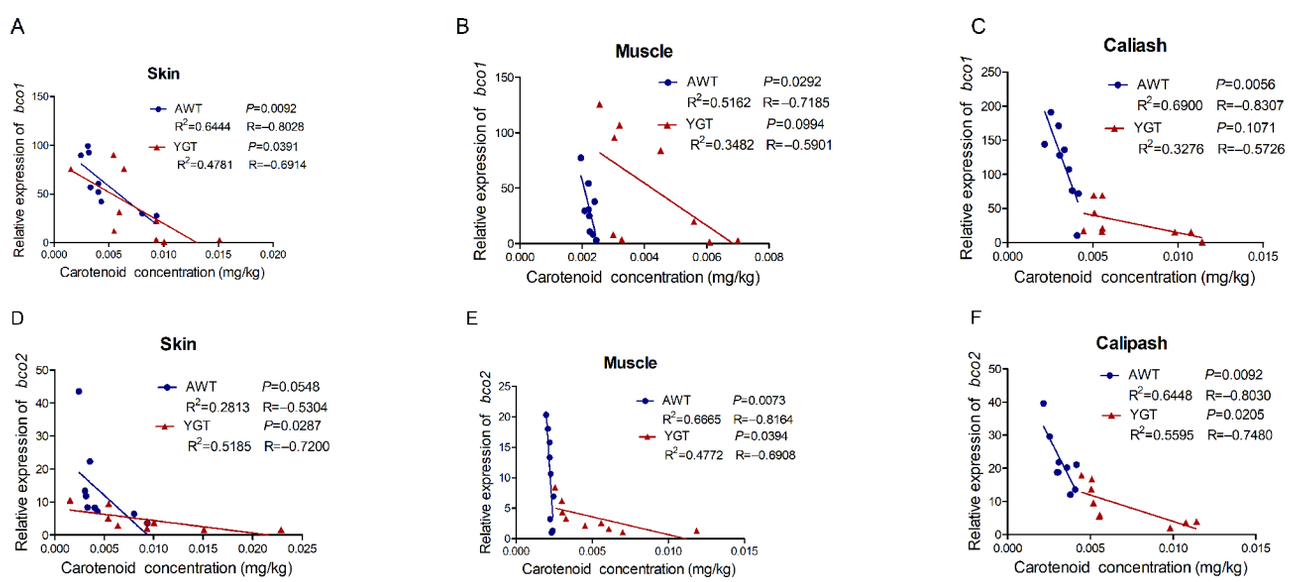

Figure 4 Correlation between carotenoid concentration and *bco1*/*bco2* expression in the skin, muscle, and calipash of Yongzhang golden turtles (YGTs) and atrovirens wild-type turtles (AWTs)

A–C: Correlation between carotenoid concentration and relative *bco1* expression in skin, muscle, and calipash. D–F: Correlation between carotenoid concentration and relative *bco2* expression in skin, muscle, and calipash.

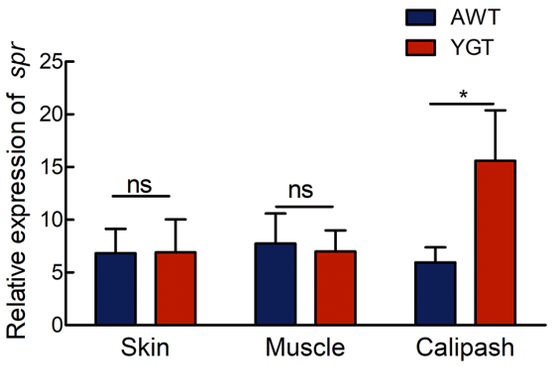

Figure 5 Comparison of relative expression of *spr* in skin, muscle, and calipash between atrovirens wild-type turtles (AWTs) and Yongzhang golden turtles (YGTs)

Figure shows mean±SE. ns: Not significant; *: P<0.05.

while down-regulation of *bco1* and *bco2*, key genes in carotenoid metabolism, facilitated carotenoid retention. Unlike in other reptiles, pterins did not play a significant role in the production of bright yellow coloration in YGTs. To the best of our knowledge, this is the first study to functionally characterize the molecular basis of yellow body coloration in turtles, with broader implications for understanding the genetic regulation of pigmentation in vertebrates.

Traditionally, reptiles were thought to lack the ability to produce pheomelanin pigments. However, recent studies identified the presence of two types of melanin, eumelanin and pheomelanin, in lacertid lizards (Megía-Palma et al., 2018). Whether reduced melanin levels contribute to yellow coloration in reptiles remains uncertain. In worm lizards (Amphisbaenia), yellow pigmentation arises from a reduction in eumelanin rather than pheomelanin (Recio et al., 2022), while in red-eared sliders (*Trachemys scripta elegans*), melanin deposition is not associated with ontogenetic color changes in the carapace (Cao et al., 2018). Our findings further support the role of reduced melanin pigmentation in the yellow phenotype of YGTs, with a single amino acid substitution in *tyrp1* identified as a key driver of this coloration. In our previous study, we detected no mutations in *tyr* or *tyrp2* but found a single mutation in *tyrp1* specific to YGTs (Wang et al., 2022). Here, to validate the functional impact of this mutation, h*tyrp1*-KO single-cell clones were generated using CRISPR/Cas9, confirming that the I481R substitution in *tyrp1* plays a central role in the reduction of melanin synthesis and formation of yellow coloration in YGTs.

Reptiles achieve their diverse red-to-yellow coloration through the deposition of carotenoid and pterin pigments, with previous studies indicating that orange pigmentation is associated with elevated pterin levels, while yellow coloration typically results from high carotenoid concentrations (Brejcha et al., 2019; De Mello et al., 2021; Olsson et al., 2013). As observed in lizards and crocodiles, turtles develop red-yellow skin pigmentation through the presence of carotenoids and/or pteridine within the dermis (Brejcha et al., 2019; Steffen et al., 2021). In this study, significant differences in carotenoid concentrations were detected between YGTs and AWTs, with YGTs exhibiting higher levels of yellow carotenoids, indicating that carotenoid accumulation plays a key role in the development of their bright yellow phenotype. Since turtles are incapable of *de novo* carotenoid biosynthesis, these pigments must be obtained from dietary components. The yellow body coloration of YGTs is likely driven by alterations in carotenoid metabolism rather than differences in dietary intake, as both YGTs and AWTs are exposed to the same dietary carotenoids. Both *bco1* and *bco2*, key genes involved in carotenoid metabolism, have been implicated in yellow pigmentation across multiple taxa (Eriksson et al., 2008; Lehnert et al., 2019; Widjaja-Adhi & Golczak, 2020). Consistent with this, YGTs exhibited significantly lower *bco1* and *bco2* expression, corresponding to reduced enzymatic activity and subsequent carotenoid accumulation. However, no coding mutations were identified in *bco1* or *bco2*, suggesting that differences in pigmentation may be controlled by variations in non-coding regulatory sequences affecting gene expression.

Pteridine pigments, including sepiapterin and xanthopterin, contribute to the production of vivid yellow, orange, and red coloration in many animals (Andrade et al., 2019; Brejcha et al., 2019; Weiss et al., 2012). In red-eared sliders and river cooters (*Pseudemys concinna*), chromatophores containing a mosaic of carotenoids, pterins, and iridophores are responsible for the yellow markings on the chin, post-orbital region, and forelimbs (Brejcha et al., 2019). However, our analysis of pigment composition in YGTs revealed no increase in total pterin, sepiapterin, or xanthopterin concentrations in the skin or muscle. In contrast, sepiapterin levels were higher in the skin of AWTs than in YGTs, while xanthopterin was exclusively detected in the skin and muscle of AWTs. Furthermore, *spr,* a key gene involved in the synthesis, transformation, and degradation of pterins, showed no significant difference in expression between YGTs and AWTs in either the skin or muscle. These findings suggest that pterins are not significantly involved in the formation of yellow body coloration in YGTs.

In conclusion, our results indicated that yellow pigmentation in YGTs resulted from a combination of reduced melanin synthesis due to an I481R mutation in *tyrp1* and increased carotenoid accumulation driven by the down-regulation of *bco1* and *bco2*. While this study followed a candidate gene approach, alternative methodologies such as genome-wide association studies (GWAS) could potentially identify additional genetic factors involved in yellow pigmentation. Nevertheless, our findings provide compelling genetic and functional evidence for the combined effects of pigments on yellow body coloration in reptiles. When considered alongside studies in other vertebrates, this work enhances our understanding of the genetic and evolutionary basis of body color variation in animals.

SUPPLEMENTARY DATA

Supplementary data to this article can be found online.

COMPETING INTERESTS

The authors declare that they have no competing interests.

AUTHORS' CONTRIBUTIONS

J.Z., X.F.W., W.G.D., and Y.Q.G. conceived and designed the experiments; J.Z., Z.H.D., and P.F.W. performed the experiments. J.Z. and X.F.W. wrote the manuscript. J.Z., X.F.W., W.G.D., and Y.Q.G. reviewed and edited the manuscript. All authors read and approved the final version of the manuscript.

ACKNOWLEDGMENTS

The authors thank Guo-Ming Cui and Yong-Zhang Han for providing the atrovirens wild-type turtles and Yongzhang golden turtles, respectively.

REFERENCES

Amengual J, Lobo GP, Golczak M, et al. 2011. A mitochondrial enzyme degrades carotenoids and protects against oxidative stress. *The FASEB Journal*, **25**(3): 948–959.

Amengual J, Widjaja-Adhi MAK, Rodriguez-Santiago S, et al. 2013. Two carotenoid oxygenases contribute to mammalian provitamin a metabolism. *Journal of Biological Chemistry*, **288**(47): 34081–34096

Andrade P, Pinho C, Pérez I de LanuzaG, et al. 2019. Regulatory changes in pterin and carotenoid genes underlie balanced color polymorphisms in the wall lizard. *Proceedings of the National Academy of Sciences of the United States of America*, **116**(12): 5633–5642.

Brejcha J, Bataller JV, Bosáková Z, et al. 2019. Body coloration and mechanisms of colour production in Archelosauria: the case of deirocheline turtles. *Royal Society Open Science*, **6**(7): 190319.

Cao DN, Gong SP, Yang JB, et al. 2018. Melanin deposition ruled out as cause of color changes in the red-eared sliders (*Trachemys scripta elegans*). *Comparative Biochemistry and Physiology Part B, Biochemistry & Molecular Biology: Biochemistry and Molecular Biology*, **217**: 79–85.

Caro T, Mallarino R. 2020. Coloration in mammals. *Trends in Ecology & Evolution*, **35**(4): 357–366.

Cloney R. 2017. Birds of a feather - genetic mapping of yellow pigmentation. *Nature Reviews Genetics*, **18**(12): 702–703.

Cooke TF, Fischer CR, Wu P, et al. 2017. Genetic mapping and biochemical basis of yellow feather pigmentation in budgerigars. *Cell*, **171**(2): 427–439. e21.

Cuthill IC, Allen WL, Arbuckle K, et al. 2017. The biology of color. *Science*, **357**(6350): eaan0221.

De Mello PLH, Hime PM, Glor RE. 2021. Transcriptomic analysis of skin color in anole lizards. *Genome Biology and Evolution*, **13**(7): evab110.

Elkin J, Martin A, Courtier-Orgogozo V, et al. 2023. Analysis of the genetic loci of pigment pattern evolution in vertebrates. *Biological Reviews*, **98**(4): 1250–1277.

Eriksson J, Larson G, Gunnarsson U, et al. 2008. Identification of the *Yellow Skin* gene reveals a hybrid origin of the domestic chicken. *PLoS Genetics*, **4**(2): e1000010.

Fu YL, Tippets CA, Donev EU, et al. 2016. Structural colors: from natural to artificial systems. *WIREs Nanomedicine and Nanobiotechnology*, **8**(5): 758–775.

Funk ER, Taylor SA. 2019. High-throughput sequencing is revealing genetic associations with avian plumage color. *The Auk*, **136**(4): ukz048.

Gao JS, Wang J, Wang WJ, et al. 2013. Isolation, purification, and identification of an important pigment, sepiapterin, from integument of the *lemon* mutant of the silkworm, *Bombyx mori*. *Journal of Insect Science*, **13**(1): 118.

Grether GF, Hudon J, Endler JA. 2001. Carotenoid scarcity, synthetic pteridine pigments and the evolution of sexual coloration in guppies (*Poecilia reticulata*). *Proceedings of the Royal Society B: Biological Sciences*, **268**(1473): 1245–1253.

Hoekstra HE. 2006. Genetics, development and evolution of adaptive pigmentation in vertebrates. *Heredity*, **97**(3): 222–234.

Hosoi J, Abe E, Suda T, et al. 1985. Regulation of melanin synthesis of B16 mouse melanoma cells by 1α, 25-dihydroxyvitamin D_3 and retinoic acid. *Cancer Research*, **45**(4): 1474–1478.

Hubbard JK, Uy JAC, Hauber ME, et al. 2010. Vertebrate pigmentation: from underlying genes to adaptive function. *Trends in Genetics*, **26**(5): 231–239.

Ito S, Wakamatsu K. 2003. Quantitative analysis of eumelanin and pheomelanin in humans, mice, and other animals: a comparative review. *Pigment Cell Research*, **16**(5): 523–531.

Kelsh RN, Harris ML, Colanesi, S, et al. 2009. Stripes and belly-spots—a review of pigment cell morphogenesis in vertebrates. *Seminars in Cell & Developmental Biology*, **20**(1): 90–104.

Lehnert SJ, Christensen KA, Vandersteen WE, et al. 2019. Carotenoid pigmentation in salmon: variation in expression at *BCO2–1* locus controls a key fitness trait affecting red coloration. *Proceedings of the Royal Society B: Biological Sciences*, **286**(1913): 20191588

Lu B, Qiu X, Yang WZ, et al. 2024. Genetic basis and evolutionary forces of sexually dimorphic color variation in a toad-headed agamid lizard. *Molecular Biology and Evolution*, **41**(3): msae054.

Macedonia JM, James S, Wittle LW, et al. 2000. Skin pigments and coloration in the Jamaican radiation of Anolis lizards. *Journal of Herpetology*, **34**(1): 99–109.

Marçon CR, Maia M. 2019. Albinism: epidemiology, genetics, cutaneous characterization, psychosocial factors. *Anais Brasileiros de Dermatologia*, **94**(5): 503–520.

McGraw KJ. 2006a. Mechanics of melanin-based coloration. *In*: Hill GE, McGraw KJ. Bird Coloration: Mechanisms and Measurements. Cambridge: Harvard University Press, 243–294.

McGraw KJ. 2006b. Mechanics of uncommon colors: Pterins, porphyrins, and psittacofulvins. *In*: Hill GE, McGraw KJ. Bird Coloration: Mechanisms and Measurements. Cambridge: Harvard University Press, 354–398.

McGraw KJ. 2006c. Mechanics of carotenoid-based coloration. *In*: Hill GE, McGraw KJ. Bird Coloration: Mechanisms and Measurements. Cambridge: Harvard University Press, 177–242.

McGraw KJ, Hill GE, Navara KJ, et al. 2004. Differential accumulation and pigmenting ability of dietary carotenoids in colorful finches. *Physiological and Biochemical Zoology*, **77**(3): 484–491.

McLean CA, Lutz A, Rankin KJ, et al. 2017. Revealing the biochemical and genetic basis of color variation in a polymorphic lizard. *Molecular Biology and Evolution*, **34**(8): 1924–1935.

McLean CA, Lutz A, Rankin KJ, et al. 2019. Red carotenoids and associated gene expression explain colour variation in frillneck lizards. *Proceedings of the Royal Society B: Biological Sciences*. **286**(1907): 20191172.

Megía-Palma R, Jorge A, Reguera S. 2018. Raman spectroscopy reveals the presence of both eumelanin and pheomelanin in the skin of lacertids. *Journal of Herpetology*, **52**(1): 67–73.

Merkling T, Chandrasoma D, Rankin KJ, et al. 2018. Seeing red: pteridine-based colour and male quality in a dragon lizard. *Biological Journal of the Linnean Society*, **124**(4): 677–689.

Mills MG, Patterson LB. 2009. Not just black and white: pigment pattern development and evolution in vertebrates. *Seminars in Cell & Developmental Biology*, **20**(1): 72–81.

Olsson M, Stuart-Fox D, Ballen C. 2013. Genetics and evolution of colour patterns in reptiles. *Seminars in Cell & Developmental Biology*, **24**(6-7): 529–541.

Orteu A, Jiggins CD. 2020. The genomics of coloration provides insights into adaptive evolution. *Nature Reviews Genetics*, **21**(8): 461–475.

Ozeki H, Ito S, Wakamatsu K, et al. 1995. Chemical characterization of hair melanins in various coat-color mutants of mice. *Journal of Investigative Dermatology*, **105**(3): 361–366.

Plotkin M, Volynchik S, Ermakov NY, et al. 2009. Xanthopterin in the oriental hornet (*Vespa orientalis*): light absorbance is increased with maturation of yellow pigment granules. *Photochemistry and Photobiolog*, **85**(4): 955–961.

Ready ZC, Keller K. 2023. Transmucosal pentobarbital is a successful euthanasia method in pond slider turtles (*Trachemys scripta*). *American Journal of Veterinary Research*, **84**(7): 1–8.

Recio P, Rodríguez-Ruiz G, López P, et al. 2022. Size-related changes and chemical basis of melanin-based body coloration in the amphisbaenian *Trogonophis wiegmanni*. *Amphibia-Reptilia*, **43**(4): 369–377.

Recknagel H, Leitão HG, Elmer KR. 2024. Genetic basis and expression of

ventral colour in polymorphic common lizards. *Molecular Ecology*, **33**(5): e17278

Roulin A, Ducrest AL. 2013. Genetics of colouration in birds. *Seminars in Cell & Developmental Biology*, **24**(6-7): 594–608.

San-Jose LM, Roulin A. 2017. Genomics of coloration in natural animal populations. *Philosophical Transactions of the Royal Society B: Biological Sciences*, **372**(1724): 20160337.

Saranathan V, Finet C. 2021. Cellular and developmental basis of avian structural coloration. *Current Opinion in Genetics & Development*, **69**: 56–64.

Schartl M, Larue L, Goda M, et al. 2016. What is a vertebrate pigment cell?. *Pigment Cell & Melanoma Research*, **29**(1): 8–14.

Shawkey MD, D'Alba L. 2017. Interactions between colour-producing mechanisms and their effects on the integumentary colour palette. *Philosophical Transactions of the Royal Society B: Biological Sciences*, **372**(1724): 20160536.

Singh A, Nüsslein-Volhard C. 2015. Zebrafish stripes as a model for vertebrate colour pattern formation. *Current Biology*, **25**(2): R81–R92.

Slominski A, Tobin DJ, Shibahara S, et al. 2004. Melanin pigmentation in mammalian skin and its hormonal regulation. *Physiological Reviews*, **84**(4): 1155–1228.

Steffen JE, Hultberg J, Drozda S. 2019. The effect of dietary carotenoid increase on painted turtle spot and stripe color. *Comparative Biochemistry and Physiology Part B: Biochemistry and Molecular Biology*, **229**: 10–17.

Steffen JE, McGraw KJ. 2007. Contributions of pterin and carotenoid pigments to dewlap coloration in two anole species. *Comparative Biochemistry and Physiology Part B: Biochemistry and Molecular Biology*, **146**(1): 42–46.

Steffen JE, McGraw KJ. 2009. How dewlap color reflects its carotenoid and pterin content in male and female brown anoles (*Norops sagrei*). *Comparative Biochemistry and Physiology Part B: Biochemistry and Molecular Biology*, **154**(3): 334–340.

Steffen JE, Quigley R, Whibley I, et al. 2021. Carotenoid deprivation and beta-carotene's effects on male and female turtle color. *Comparative Biochemistry and Physiology Part B: Biochemistry and Molecular Biology*, **253**: 110546

Sun BJ, Li WM, Lv P, et al. 2024. Genetically encoded lizard color divergence for camouflage and thermoregulation. *Molecular Biology and Evolution*, **41**(2): msae009.

Tang CY, Zhang XH, Xu X, et al. 2023. Genetic mapping and molecular mechanism behind color variation in the Asian vine snake. *Genome Biology*, **24**(1): 46.

Tian X, Shan YS, Peng NN, et al. (2024). Sepiapterin reductase (Spra and Sprb) regulate carotenoid and pteridine metabolism influencing the koi carp (*Cyprinus carpio* L.) coloration. *Aquaculture Reports*, **34**: 101900.

Wang YG, Zhang J, Liu WT, et al. 2022. Morphological and molecular biological characterization of the Yongzhang golden turtle, a new strain of *Pelodiscus sinensis*. *Aquaculture*, **548**: 737536.

Weiss SL, Foerster K, Hudon J. 2012. Pteridine, not carotenoid, pigments underlie the female-specific orange ornament of striped plateau lizards (*Sceloporus virgatus*). *Comparative Biochemistry and Physiology Part B: Biochemistry and Molecular Biology*, **161**(2): 117–123.

Widjaja-Adhi MAK, Golczak M. 2020. The molecular aspects of absorption and metabolism of carotenoids and retinoids in vertebrates. *Biochimica et Biophysica Acta (BBA) - Molecular and Cell Biology of Lipids*, **1865**(11): 158571

Wolff GL. 2003. Regulation of yellow pigment formation in mice: a historical perspective. *Pigment Cell Research*, **16**(1): 2–15.

Zhang J, Ding ZH, Du WG, et al. 2023. Carotenoids act on coloration and increase immunity and antioxidant activity in the novel "Yongzhang golden turtle" strain of *Pelodiscus sinensis*. *Aquaculture*, **563**: 738871.

Ziegler I. 2003. The pteridine pathway in zebrafish: regulation and specification during the determination of neural crest cell-fate. *Pigment Cell Research*, **16**(3): 172–182.